NASA TECHNICAL NOTE

NASA TN D-2183

PERFORMANCE CHARACTERISTICS OF A PREFORMED ELLIPTICAL PARACHUTE AT ALTITUDES BETWEEN 200,000 AND 100,000 FEET OBTAINED BY IN-FLIGHT PHOTOGRAPHY

by Charles H. Whitlock and Harold N. Murrow

Langley Research Center
Langley Station, Hampton, Va.

NATIONAL AERONAUTICS AND SPACE ADMINISTRATION • WASHINGTON, D. C. • FEBRUARY 1964

PERFORMANCE CHARACTERISTICS OF A PREFORMED ELLIPTICAL PARACHUTE AT ALTITUDES BETWEEN 200,000 AND 100,000 FEET OBTAINED BY IN-FLIGHT PHOTOGRAPHY

By Charles H. Whitlock and Harold N. Murrow

Langley Research Center
Langley Station, Hampton, Va.

NATIONAL AERONAUTICS AND SPACE ADMINISTRATION

For sale by the Office of Technical Services, Department of Commerce,
Washington, D.C. 20230 -- Price $0.75

PERFORMANCE CHARACTERISTICS OF A PREFORMED ELLIPTICAL PARACHUTE AT ALTITUDES BETWEEN 200,000 AND 100,000 FEET OBTAINED BY IN-FLIGHT PHOTOGRAPHY

By Charles H. Whitlock and Harold N. Murrow

SUMMARY

The performance characteristics of a preformed elliptical parachute at altitudes between 200,000 and 100,000 feet have been obtained by means of in-flight photography. It was demonstrated that this type of parachute will open at altitudes of about 200,000 feet if conditions such as twisting of the suspension lines or draping of the suspension lines over the canopy do not occur. Drag-coefficient values between 0.6 and 0.8 were found to be reasonable for this type of parachute system in the altitude range between 200,000 and 100,000 feet.

INTRODUCTION

Throughout aviation history man has been interested in the parachute as a means of deceleration. More recently parachutes have been applied to the field of space research both as an aid to recovery operations and as a means of obtaining meteorological data. The usual method of performing the latter operation is to eject a meteorological sensor from a rocket vehicle at the apogee of the trajectory and then slowly to lower the sensor by parachute through the upper atmospheric region. Atmospheric properties including wind data are usually obtained during this type of descent.

One of the basic problems in obtaining data by this method is that of being able to predict parachute inflation and stability characteristics at altitudes above 100,000 feet. The Langley Research Center has undertaken an investigation into this problem of parachute performance in an effort to provide useful information for application to present and future meteorological sounding-rocket systems.

The present tests were conducted to obtain the performance characteristics of a parachute which is a component of an existing meteorological system. This system basically consists of a long slender solid-propellant rocket vehicle which boosts a payload to altitudes above 200,000 feet. A temperature sensor is then separated from the vehicle and lowered to earth by means of a preformed elliptical parachute. This particular parachute was chosen for testing because large

differences were noted between values of predicted and flight descent velocities, particularly at altitudes above 100,000 feet. As pointed out in reference 1, experimental descent velocities were much higher than velocities indicated by analytical predictions. The reasons for these discrepancies were unknown, although it was shown in the reference that the most probable reason for error might be that either (1) the parachute was not completely inflating at the higher altitudes or (2) there was an inaccurate estimate of drag variation. The purpose of these tests was to determine actual parachute inflation characteristics and drag variations from both in-flight and ground support data. In order to gather this information, the parachute opening sequence and subsequent motions were photographed by means of a recoverable camera package substituted in place of the usual temperature sensing instrument. The purpose of this report is to present both canopy inflation data and computed drag coefficients from three successful launchings with camera packages.

TEST PARACHUTE

The parachutes tested were of a preformed elliptical configuration, were 15 feet in diameter when fully inflated, and were partially silverized for radar-tracking purposes. The same type of parachute used in these tests is shown in figure 1. Details of the parachute construction, including the canopy gore pattern, and the viewing angle of the camera lens are also shown in the figure. Important parachute specifications are given in the following table:

Parachute type	Preformed elliptical
Diameter, ft	15
Weight, lb	2
Canopy material (22 percent silverized)	3-momme silk
Permeability (cu ft/min airflow per sq ft canopy area at 1/2 in. H_2O):	
White portion	600 ± 150
Silverized portion	475 ± 150
Number of gores	12
Number of suspension lines	24
Suspension-line material	Nylon
Length of suspension lines, ft	28
Length of riser line, in.	24
Parachute pack material	Lightweight canvas

In general, the parachutes were packed in a four-petal canvas bag which was positioned between two fiber-glass staves inside a 4.5-inch-diameter cylindrical metal container approximately 11.5 inches in length. Components of the parachute package are shown in figure 2 which is a four-step sequence describing parachute deployment. The parachute container is attached to the forward end of the launch vehicle immediately forward of a gas-generator separation device. (See fig. 3.) At a given time, the gas generator fires and builds up a high pressure behind the aft bulkhead (fig. 2(d)) which in turn forces the fiber-glass staves forward,

thereby shearing the attachment pins for the forward bulkhead; the sequence at this point is shown in figure 2(a). Note the lanyard in figure 2(a) which normally is attached to the launch vehicle. The parachute, canvas bag, and fiber-glass staves are ejected from the forward end of the cylindrical container. The fiber-glass staves fall free and the 2-pound break cord, shown in figure 2(c), assists in unfolding the parachute canopy before the lanyard becomes taut, thus severing the break cord. For these tests, the forward bulkhead was deleted and the parachute riser line was attached to the aft portion of the camera package.

PAYLOAD DESCRIPTION

In order to meet the objectives of this experiment, the photographic scheme shown in the descent configuration of figure 1 was used. The physical and aerodynamic properties of the existing meteorological system were simulated as closely as possible with available hardware. Estimates of the environment encountered by a payload were obtained from launch-vehicle performance estimates and the few experimental measurements available. On the basis of these estimates, the camera package shown in figure 4 was constructed.

Basically, the payload was a slender tangent-ogive-shaped camera package attached forward of the cylindrical parachute container. (See fig. 3.) The camera package consisted of a monocoque structure housing an instrumentation system which contained a camera, batteries, and activation switch. The structure was made of a phenolic nylon shell shielded against aerodynamic heating by a protective coating. The photography system used an NASA modified Air Force N-9 type 16-mm camera powered by batteries. The camera was qualified for operation under an acceleration of 50g in all directions and the camera package was undamaged by 70g shocks in the longitudinal axis direction. The camera package was also dynamically balanced at the anticipated spin rate. The film utilized was a high-speed extra-thin-base type and the cameras were operated at 16 frames per second with a shutter setting of 1/1500 second. Wide angle lenses (f/11) were utilized for the three flights (120° on flights A and B and 90° on flight C). Approximately 3 minutes of film records per flight were available from this camera system. One of the camera packages at recovery is shown in figure 5.

The total payload weight was approximately 13.1 pounds, which consisted of a 9-pound camera package, a 2-pound parachute, and a 2.1-pound parachute compartment, and compares with the 12-pound total payload weight during ascent of the existing meteorological system. During descent, the 9-pound suspended weight of the camera package, as compared with the 4.75-pound suspended weight of the meteorological sensor, was not expected to affect the parachute deployment sequence. This heavier weight, however, could affect stability of the descending system and would, of course, increase the descent velocity.

TEST RESULTS AND DISCUSSION

Operations and Vehicle Performance

The flight tests were conducted at the small missile range of the White Sands Missile Range, New Mexico. Figure 6 shows both altitude and velocity time histories for the ascent phase of the three flights. The rocket vehicles were launched at an elevation angle of 83°, burned for approximately 30 seconds, and subsequently coasted to apogee. Near apogee, the separation sequence occurred and the parachute was subjected to the environment given in the following table:

Flight	Altitude, ft	Velocity, fps	Dynamic pressure, lb/sq ft
A . . .	223,000	650	0.057
B . . .	219,500	600	0.052
C . . .	207,000	800	0.151

The environmental differences between the three flights were within expected limits for launch vehicles of this type and were not expected to affect the experimental analysis.

Parachute Performance

Descent time histories of altitude and total velocity are given in figure 7 for the three flights. For flight B, reduced radar data were not available for the first 94 seconds following separation. Consequently, the altitude and velocity data for this region (fig. 7) were estimated from plotting-board records. The low values of total velocity for flights A and C at about 16 seconds may probably be attributed to apogee conditions. From these minima the velocities increased until terminal velocity was attained at approximately 40 to 50 seconds after separation.

Figures 8(a) to 8(c) present sample photographs from each of the flights at various altitudes. Also shown for comparison purposes are photographs of the parachute in the full-open configuration, which were obtained from helicopter drop tests near sea level. These photographs show the parachute canopy with its silverized gores inside a circular field of view. The riser line projects from the left border of the pictures and extends toward the parachute canopy because of its relative position with the camera lens as shown in figure 5. From flights B and C both the sun and horizon may be seen clearly; however, this is not possible in pictures from flight A because the lens became fogged, possibly due to residue from the separation device. Fortunately, the shadow of the riser line across the lens at frequent intervals allows the canopy to be viewed. Other prominent images that can be seen in these photographs are (1) a smudge on the lens for flight B, (2) some tissue paper, used as lens protection, adhering to the riser line in flight C, and (3) clouds in the background for the sea-level

conditions. The photographs presented are an attempt to show typical frames from the flight films, but in some instances fluctuations in the canopy were quite rapid and thus made a "typical" frame somewhat difficult to present.

To determine the amount of parachute inflation, individual frames from the flight films were analyzed and the projected area was evaluated and compared with that of the full-open parachute obtained from helicopter drop tests with identical payloads. The results are shown in figure 9 where variation of the canopy projected area is shown as a percent of maximum (full open) projected area over the altitude range where photographs were obtained. It is estimated that the parachute area could be determined within an accuracy of the order of 10 percent due to lens distortion and nonuniform canopy shape. In viewing the films, it was observed that fluctuations of the canopy, commonly called "breathing," occurred at all altitudes. This condition was variable and more violent at some times than others. The bands in figure 9 represent envelopes which encompass the projected area oscillations (sometimes within experimental accuracy).

For flight A the parachute apparently remained completely open after initial oscillations were damped out. A twisting oscillation was observed although it was not severe enough to affect opening characteristics. This twisting motion was advantageous for analysis of flight A since the lens was apparently fogged by gases from the separation device. As the camera package twisted, a shadow from the riser line fell across the lens and made viewing of the canopy possible (see fig. 8(a)).

For flight B the parachute experienced oscillations of the canopy area just after separation. This motion was damped out by the time an altitude of 190,000 feet was reached. The parachute remained about 10 percent open down to 170,000 feet, at which time it began to open more fully. It was about 60 percent open when the film was depleted at 123,000 feet. Further review of the motion pictures indicated that, as the parachute began to open, the spin rate of the camera package apparently caused the parachute suspension lines to twist, deterring opening of the canopy. Approximately a minute later, the lines began to untwist and the parachute continued to open.

Inspection of figure 9(c) shows that, for flight C, the parachute experienced motions that were more violent and erratic than were evidenced in flights A and B. For this descent, however, it was not possible for the parachute to inflate entirely since two suspension lines were caught over the top of the canopy, as can be seen in figure 8(c). This probably accounts for the fact that this parachute was only about 70 percent open at 134,000 feet where the film ended.

An overall assessment of the three flights shows that the parachute performance was inconsistent even though physical characteristics of the camera and parachute packages were the same. In each flight canopy fluctuations were evident immediately following separation. It was also evident in all flights that a twisting of the suspension lines was experienced although the condition was more severe in flight B. Inspection of the parachutes upon recovery showed some small burn holes, indicating a need for adequate protection from burning residue caused by the pyrotechnic separation device.

Estimates of Drag Coefficient

As was discussed earlier, the discrepancies between predicted and in-flight parachute performance (particularly the descent rates) might be due to a combination of (1) the failure of the parachute to inflate properly and (2) an inaccurate estimate of parachute drag variation. From the results of these flight tests, values of the "effective" drag coefficient, C_D in the vertical direction, were calculated. These calculations were based on the assumption that the retardation force equals the effective drag force which may be expressed as follows:

$$\text{Drag} = \frac{-W}{g}\ddot{z} + W = C_D \frac{\rho}{2} V^2 S \tag{1a}$$

$$C_D = -\frac{2W(\ddot{z} - g)}{g\rho S V^2} \tag{1b}$$

where

W	weight of parachute and camera package (11 lb)
g	acceleration of gravity (assumed constant at 32.2 ft/sec^2)
$\ddot{z}$	vertical acceleration, positive downward, ft/sec^2
ρ	atmospheric density, slugs/cu ft (1962 standard atmosphere assumed)
$V = \dot{z}$	descent velocity ft/sec
S	measured projected canopy area (based on the flight film), sq ft
C_D	effective drag coefficient

The variation of descent velocity for the three flights is presented in figure 10. These data were determined from differentiation of the radar tracking positional data. Drag-coefficient calculations were initiated at altitudes where it was evident that the descending system was near terminal velocity. This was approximately 15,000 feet below apogee as shown in figure 7. Radar data were further differentiated to obtain the vertical acceleration data shown in figure 11. No data are shown for flight B due to the absence of reduced radar data. By utilizing experimental values of $\dot{z}$, $\ddot{z}$, and S, effective drag coefficients for flights A and C were determined from equations (1) and are shown in figure 12 as a function of velocity. Reference 2 indicates that this relationship is valid for parachutes. Investigation indicated that drag-coefficient variations showed no definite trend when related to Mach number. (Again, no data are presented for flight B.) The bands correspond to the canopy area variations presented in figure 9. It is believed that the drag-coefficient values obtained from flight A are representative of this type of parachute since all indications are that it apparently performed normally. Since the parachute of flight A was fully inflated when the film was expended, the assumption was made that this condition prevailed throughout the remaining portion of the descent. On the basis of this assumption

and of the utilization of radar tracking data to lower altitudes, the solid curve in figure 12 extending to lower velocities resulted.

Also shown in figure 12 by the dashed curve is a calculated drag-coefficient variation for the same type of parachute with the lighter suspended weight (4.75 pounds compared with 9 pounds for the flights presented herein). The dashed curve was computed from radar tracking data with the assumption of a fully inflated canopy for a typical flight selected from a number of flights made with the operational meteorological system.

A comparison of the solid and dashed curves shows the effective drag coefficients to be similar (between 0.6 and 0.8) at the higher velocities. A departure in the curves occurs at velocities below about 70 ft/sec. The reasons for the deviation in the dashed curve are unknown, although a possible cause may be derived from the discussion in reference 2. It is stated in this reference that a parachute will exhibit coning motion for heavy suspended weights and gliding motion (which gives higher effective drag) for lighter suspended weights. Parachutes also experience a transition from coning to gliding motion depending on stability conditions. It is known that the existing meteorological system does, in fact, experience coning at high altitudes as is shown in figure 13 in a sequence of photographs from a typical flight at the NASA Wallops Station. These pictures were taken from a ground-camera installation when the descending system was at approximately 150,000 feet. It is possible, then, that the parachute investigated herein experiences a stability transition at about 100,000 feet with the lighter suspended weight used in operational meteorological flights but had not yet reached this transition at the end of the usable radar data period which occurred at 40,000 feet for the heavy suspended weight of these tests.

CONCLUDING REMARKS

It was demonstrated that preformed elliptical parachutes will open at altitudes of about 200,000 feet if conditions such as twisting of the suspension lines or draping of the suspension lines over the canopy do not occur. From these tests, it appears that it would be desirable to reduce the initial spin rate of the package at separation from the launch vehicle and to provide a means of damping this movement after parachute deployment. The parachute performance in these tests was inconsistent because of these undesirable effects. Drag-coefficient computations, based on in-flight photographs showing area variations, indicated values between 0.6 and 0.8 for this type of parachute system, although an increase at lower altitudes may occur. Regarding high-altitude parachute performance, it would be of considerable interest to investigate further the problems of parachute deployment and transition from coning to gliding motions.

Langley Research Center,
National Aeronautics and Space Administration,
Langley Station, Hampton, Va., October 23, 1963.

REFERENCES

1. Murrow, Harold N., and Barker, Lawrence E., Jr.: An Analytical Study of the Wind-Following Characteristics of a Parachute at High Altitudes. 1961 Proc. ISA 16th Annual Instrument-Automation Conf. and Exhibit, vol. 16 - pt. II, 1961, pp. 169-LA-61-1 - 169-LA-61-8.

2. Heinrich, Helmut G.: Drag and Stability of Parachutes. Aero. Eng. Rev., vol. 15, no. 6, June 1956, pp. 73-81.

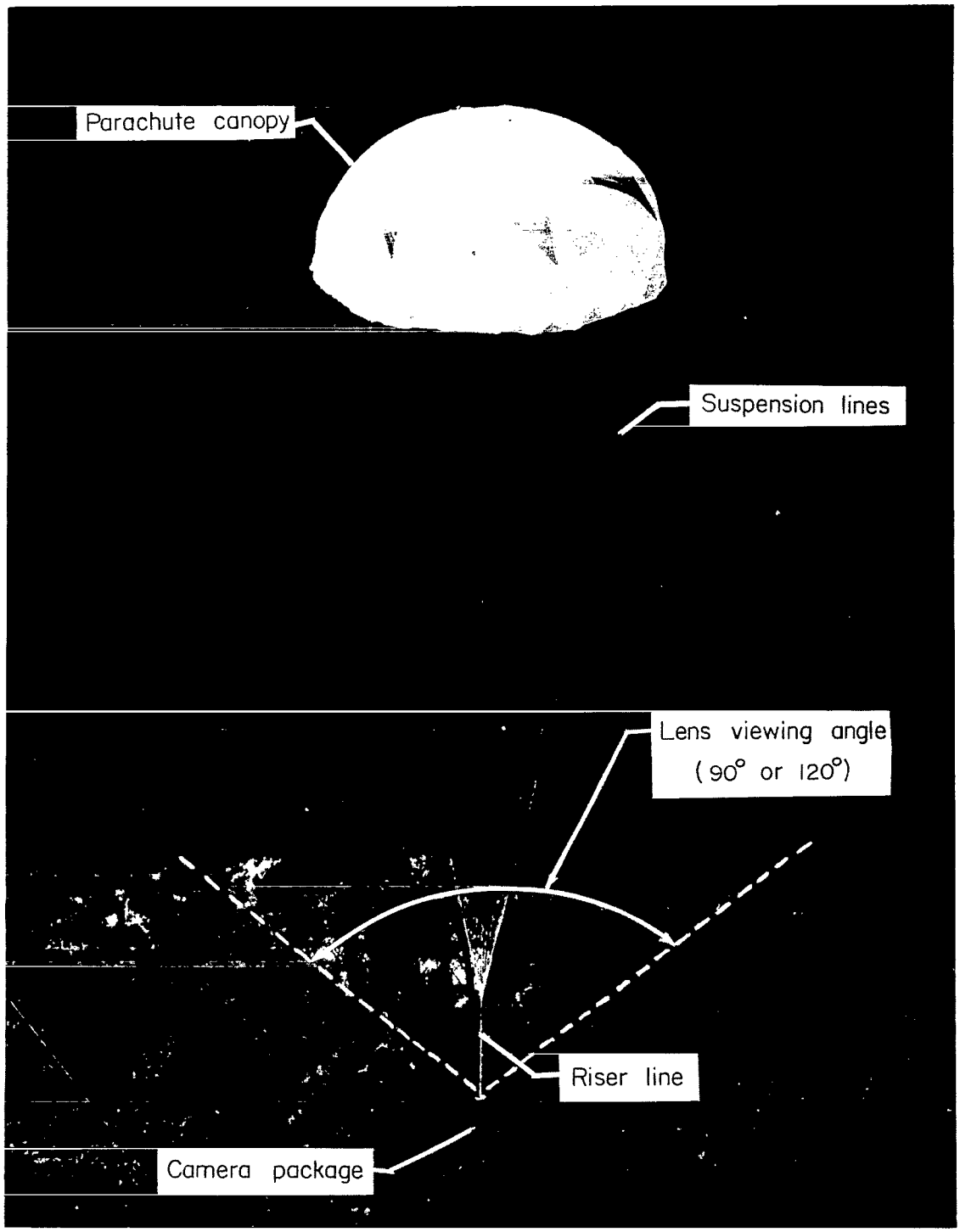

Figure 1.- Descent configuration. L-63-7516

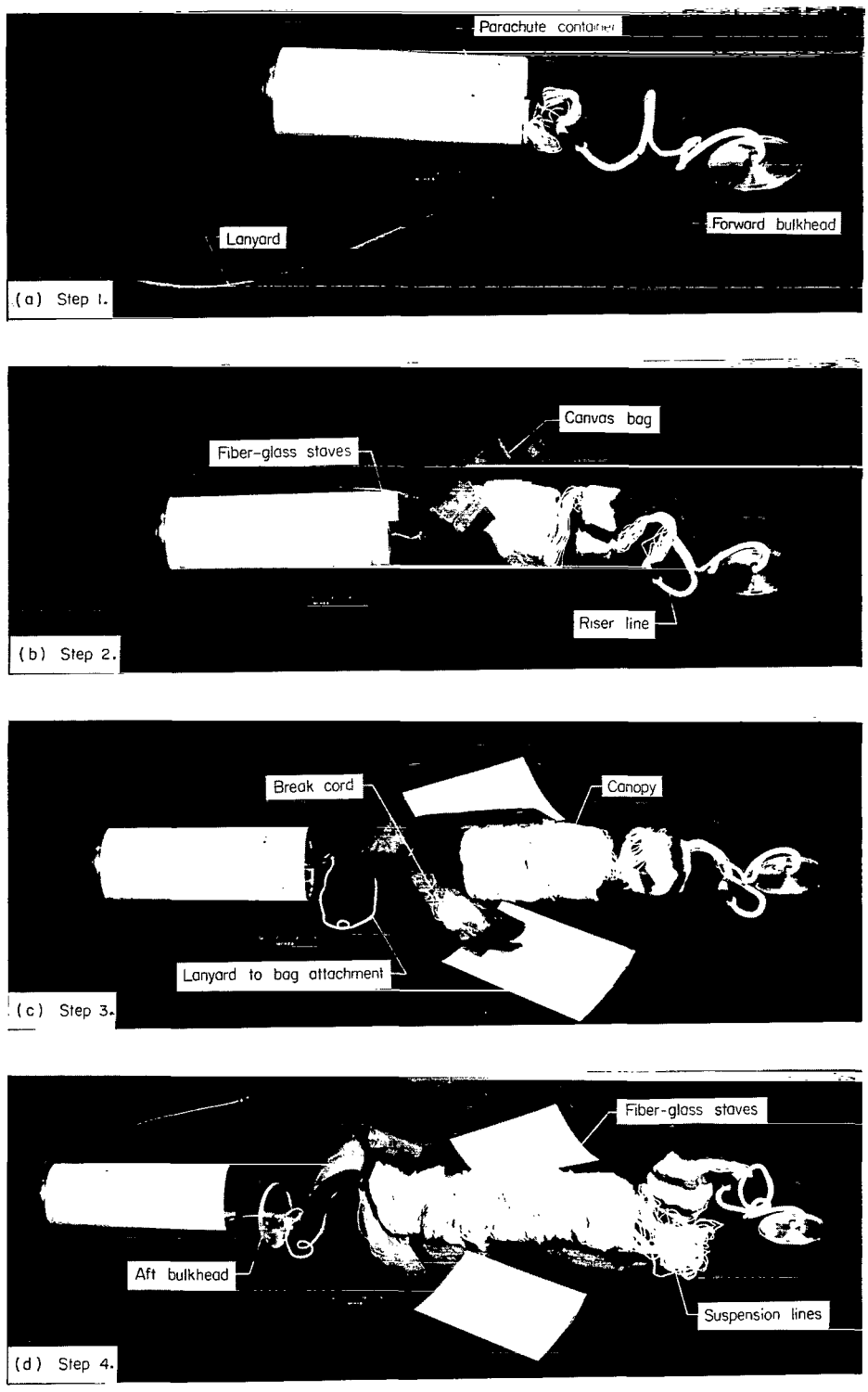

Figure 2.- Description of parachute deployment. L-63-7517

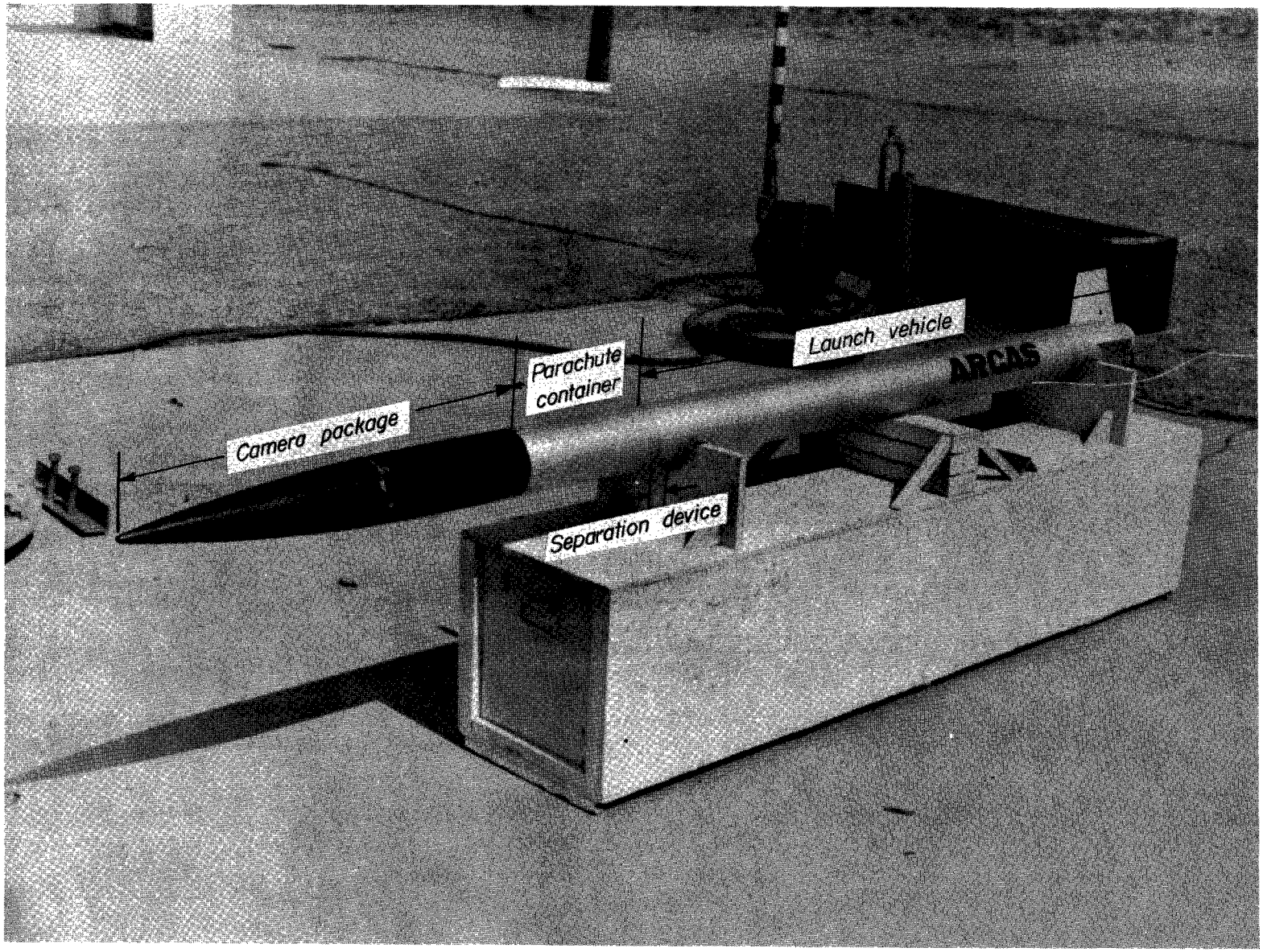

Figure 3.- Photograph of flight vehicle. (Official U.S. Army photograph.) L-63-7518

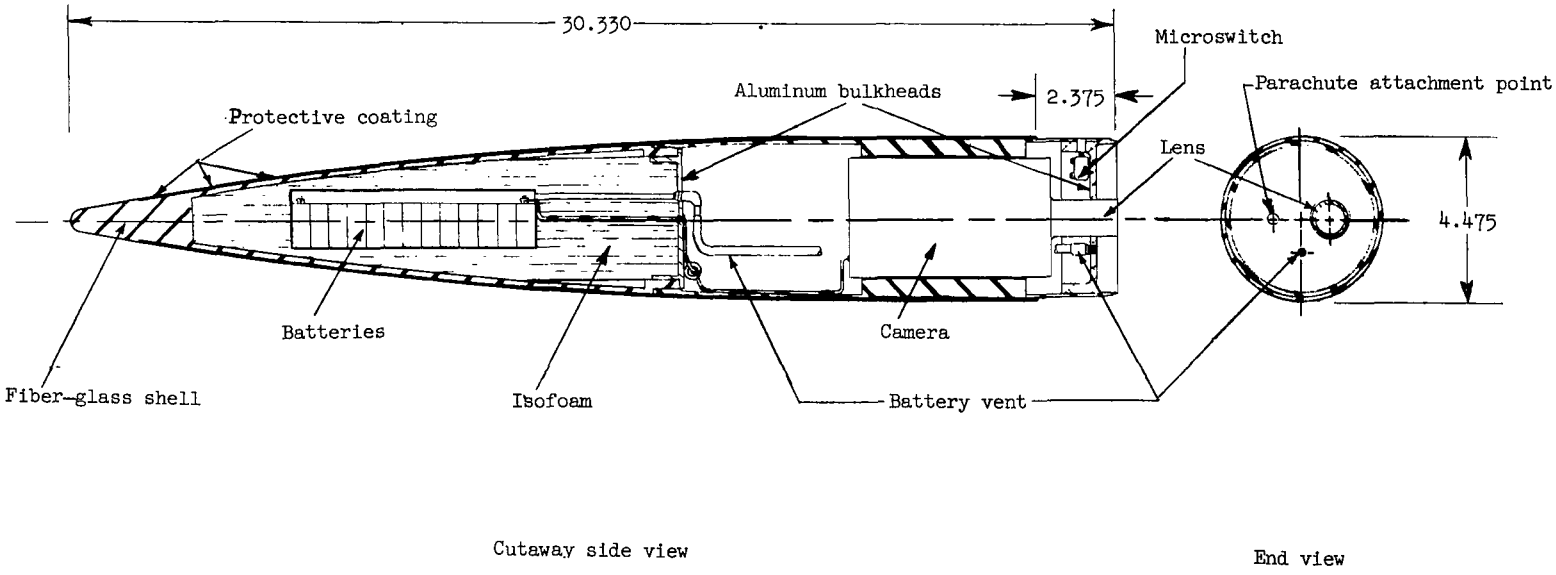

Figure 4.- Assembly drawing of camera package. Dimensions are in inches.

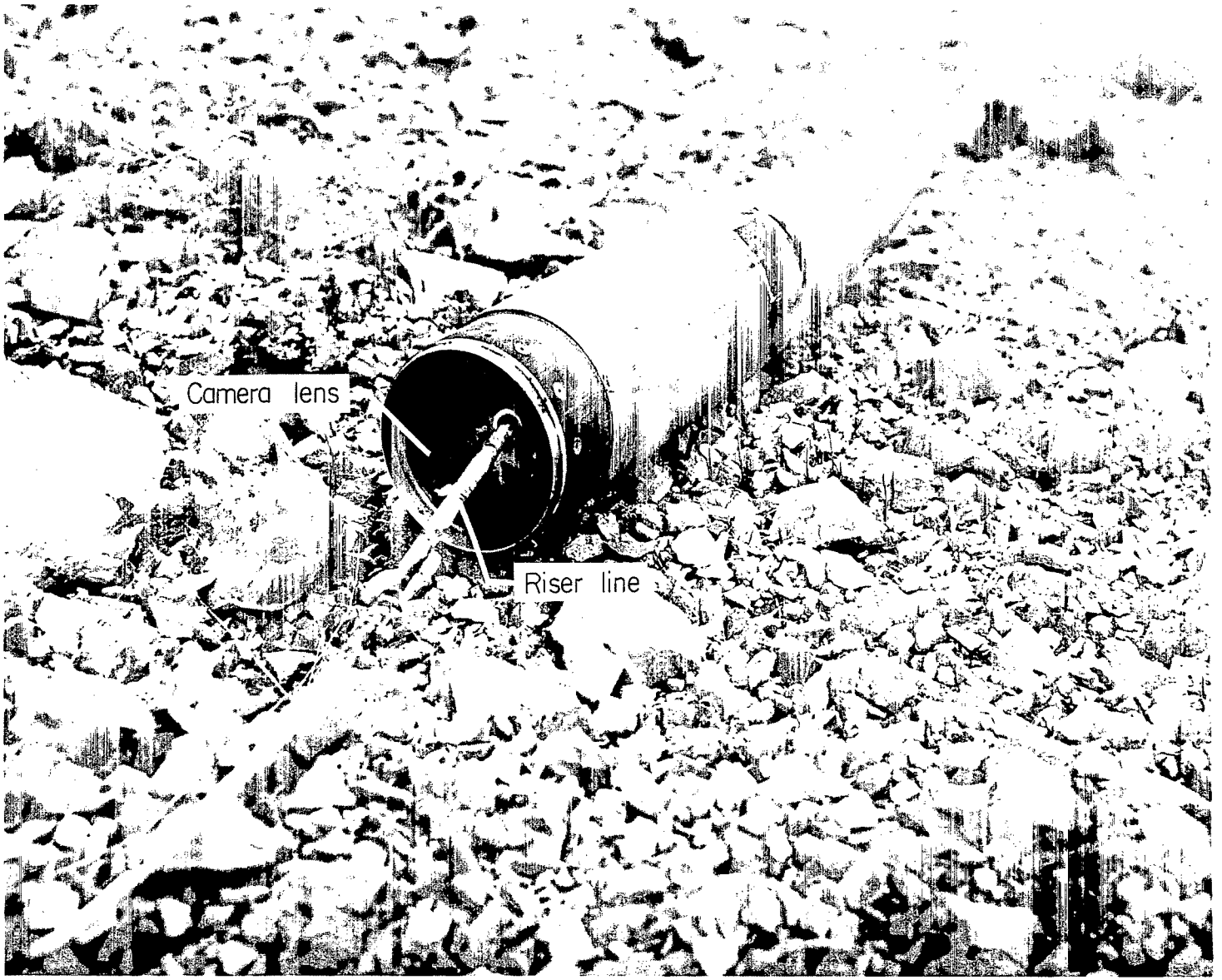

Figure 5.- Camera package at recovery. (Official U.S. Army photograph.) L-63-7519

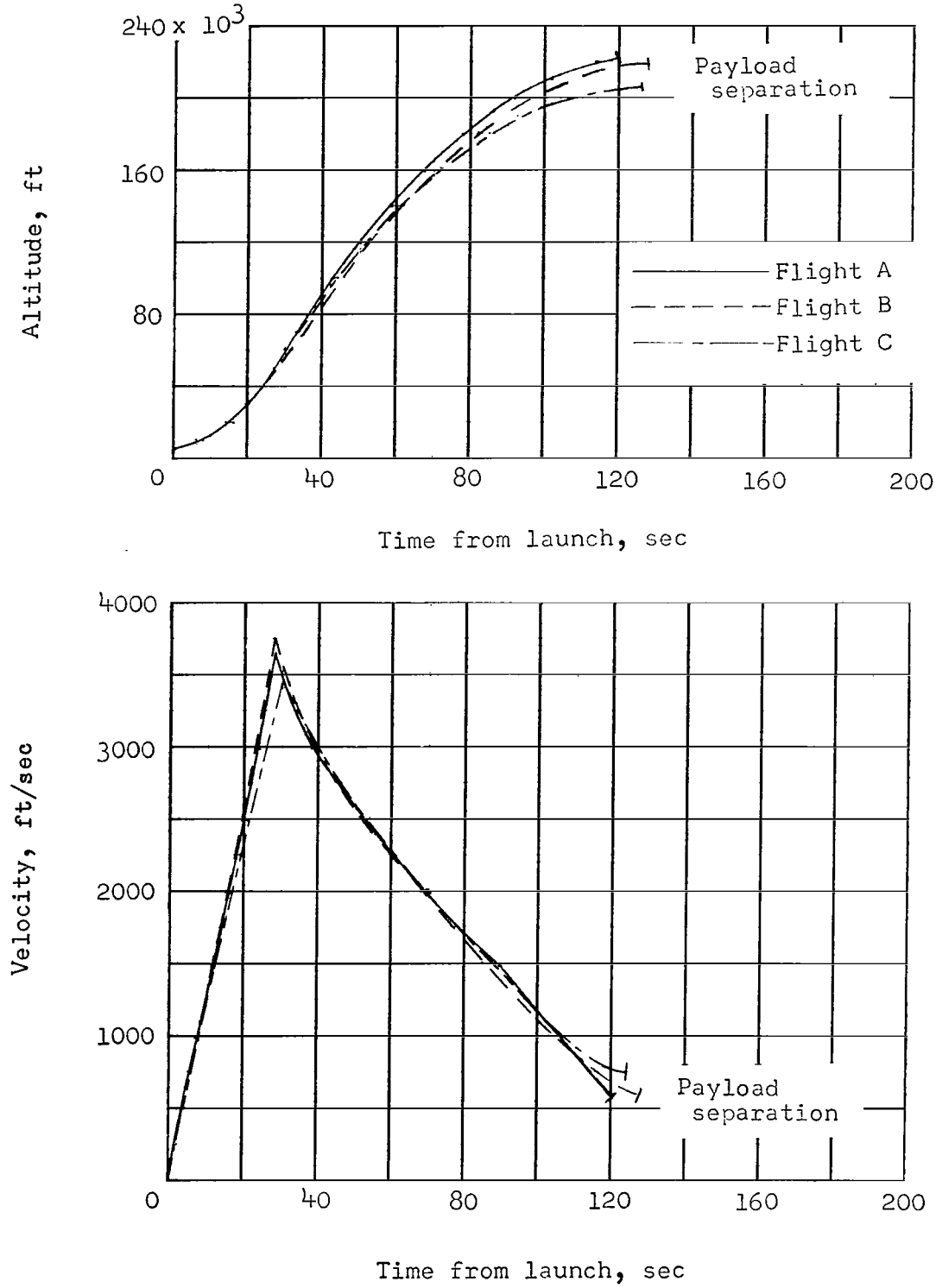

Figure 6.- Altitude and velocity time histories during ascent.

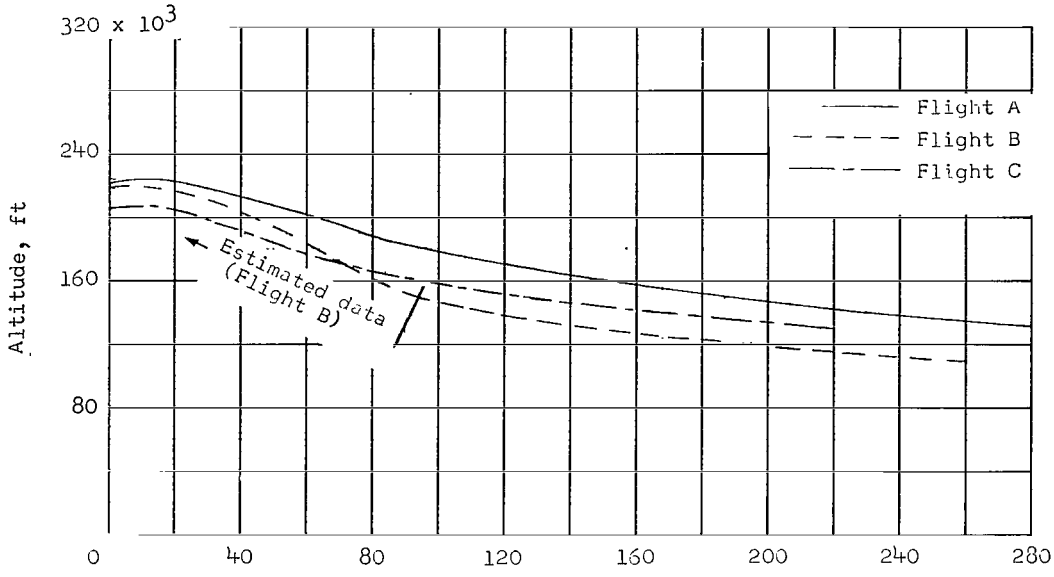

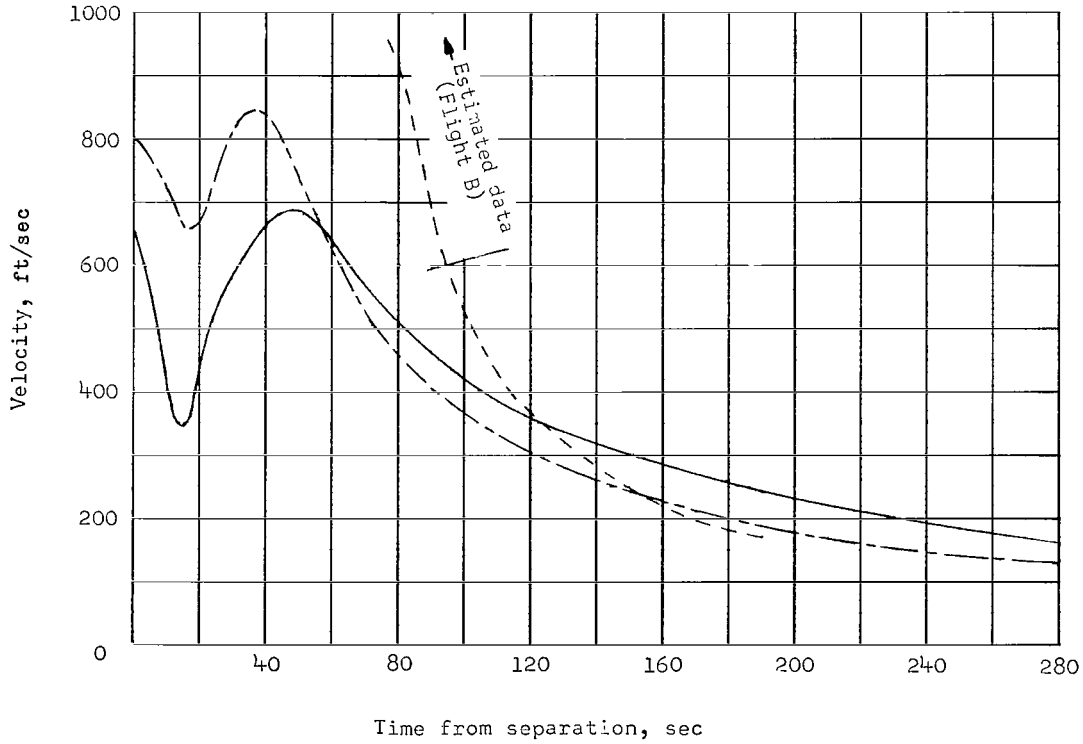

Figure 7.- Altitude and velocity time histories during descent.

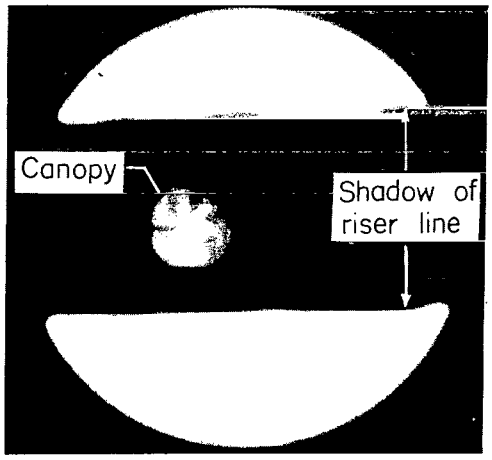

Altitude, 200,000 ft

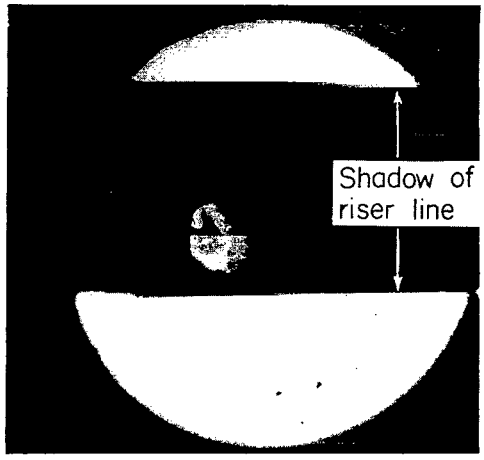

Altitude, 165,000 ft

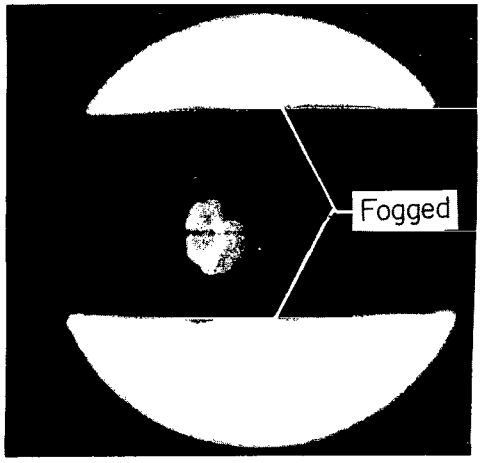

Altitude, 152,000 ft

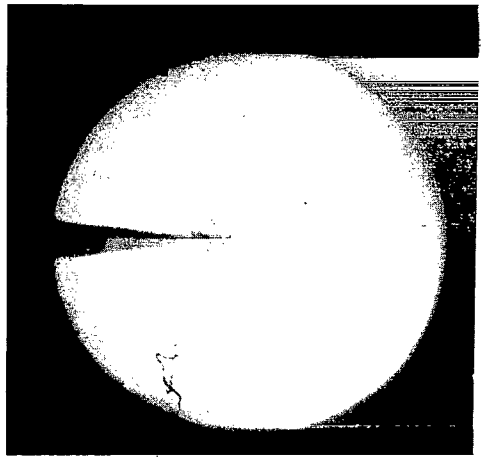

Sea level
(from helicopter drop test)

(a) Flight A (120° lens).

Figure 8.- Sample photographs from the three flights. L-63-7520

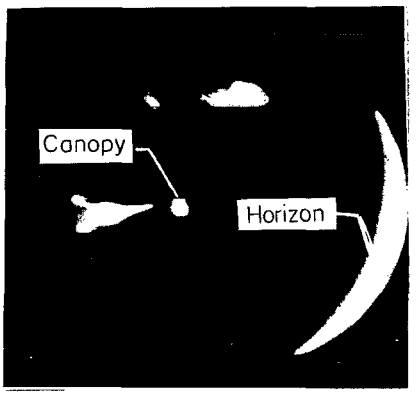

Altitude, 195,000 ft

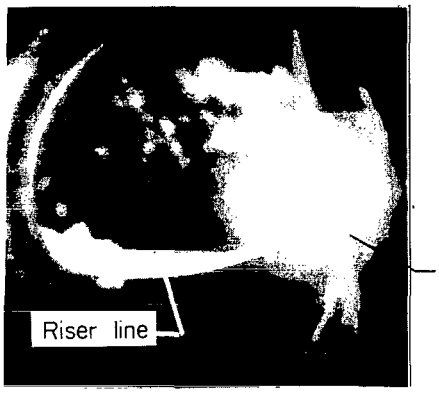

Altitude, 165,000 ft

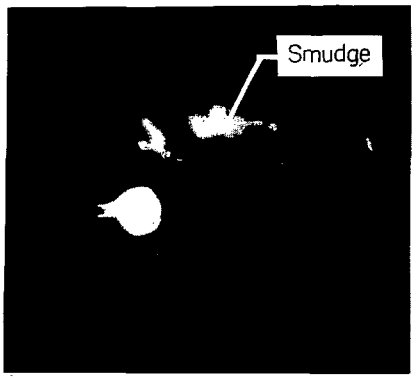

Altitude, 123,000 ft

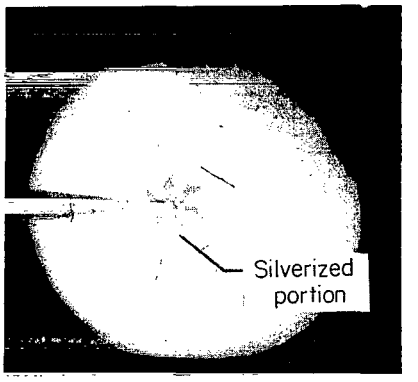

Sea level
(from helicopter drop test)

(b) Flight B (120° lens).

Figure 8.- Continued. L-63-7521

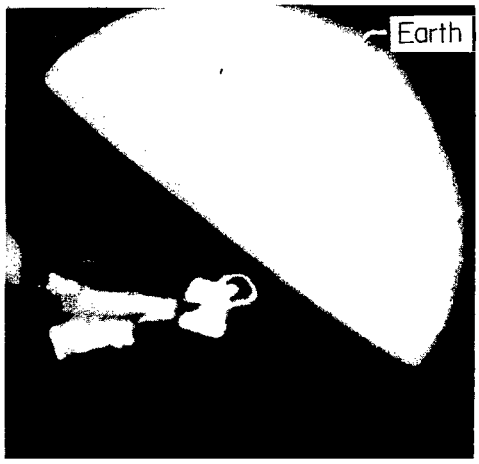

Altitude, 200,000 ft

Altitude, 165,000 ft

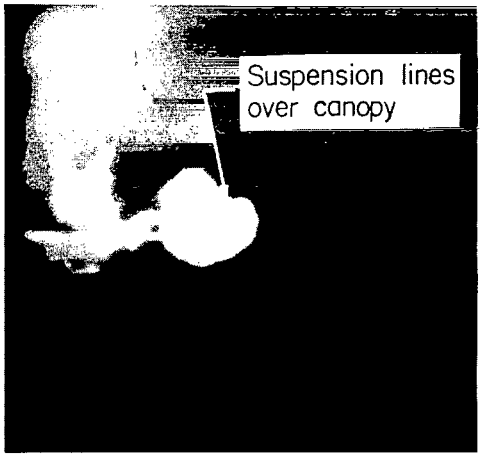

Altitude, 137,000 ft

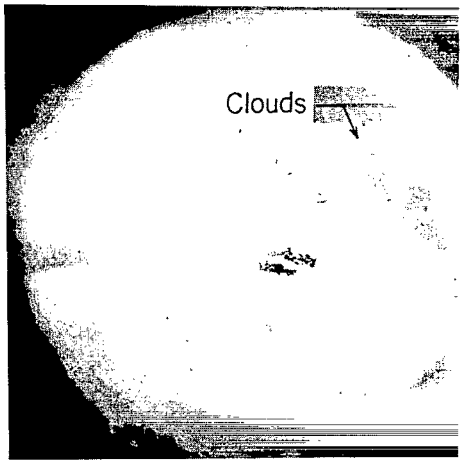

Sea level
(from helicopter drop test)

(c) Flight C (90° lens). L-63-7522

Figure 8.- Concluded.

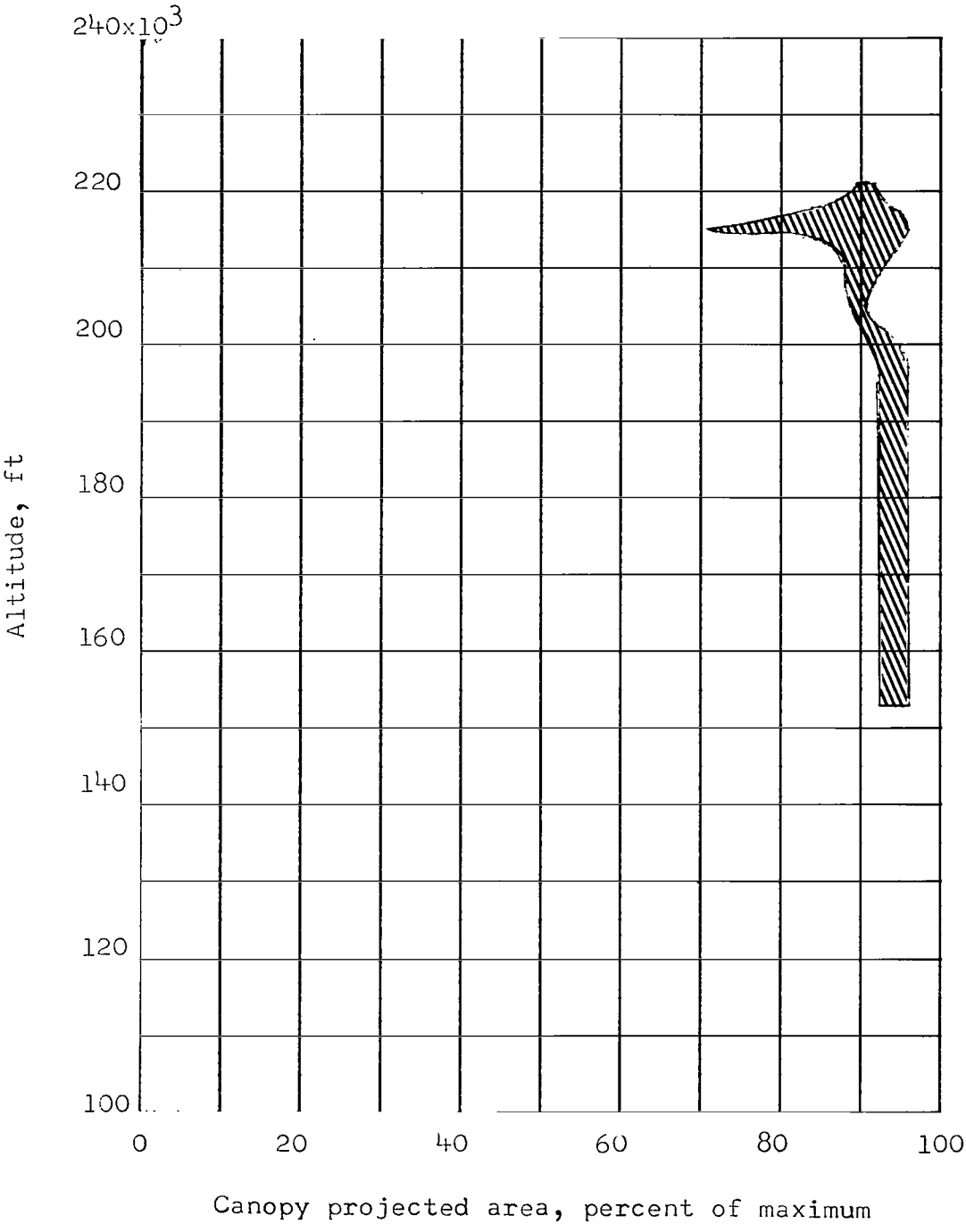

(a) Flight A.

Figure 9.- Variation of projected area for the three flights.

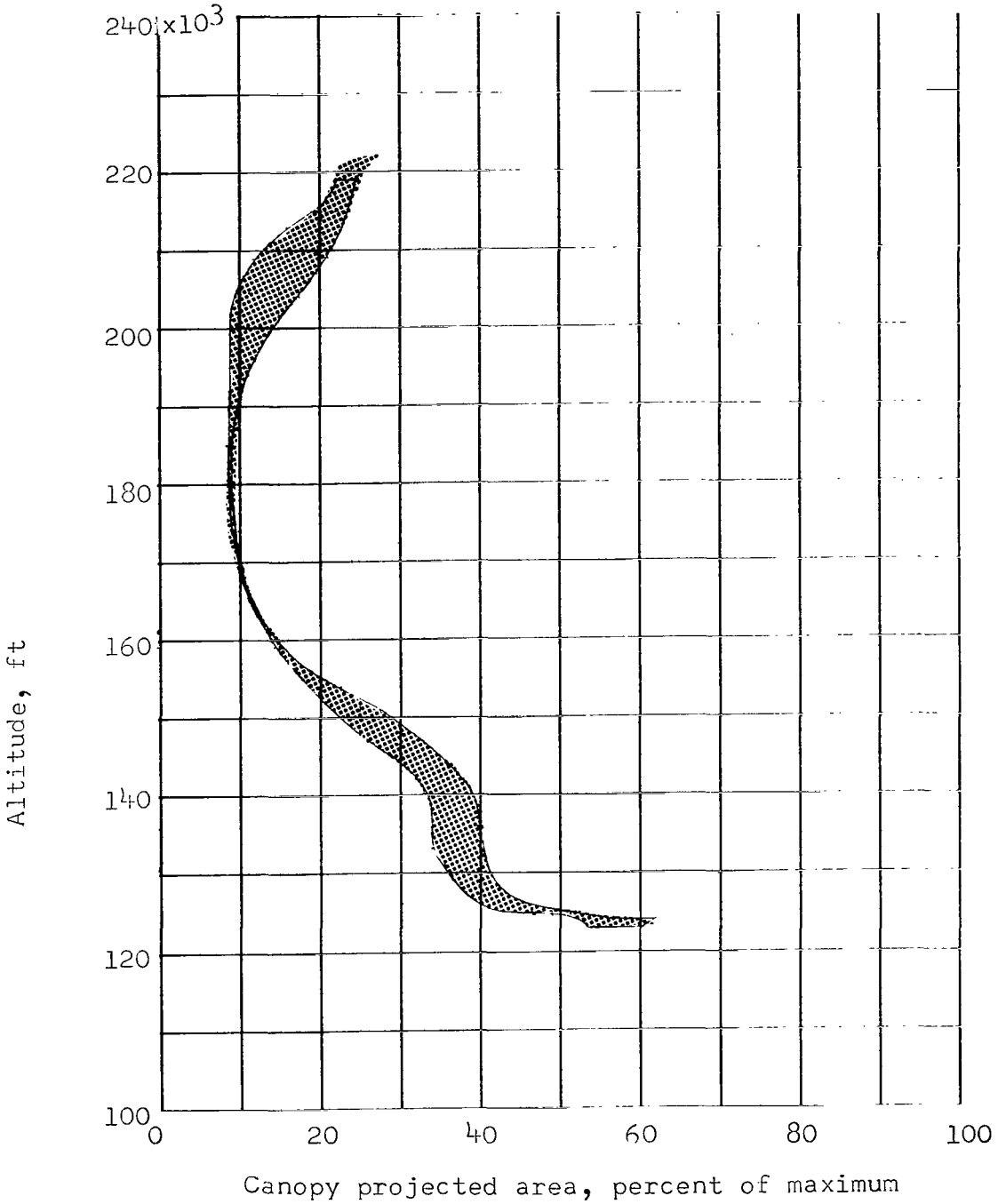

(b) Flight B.

Figure 9.- Continued.

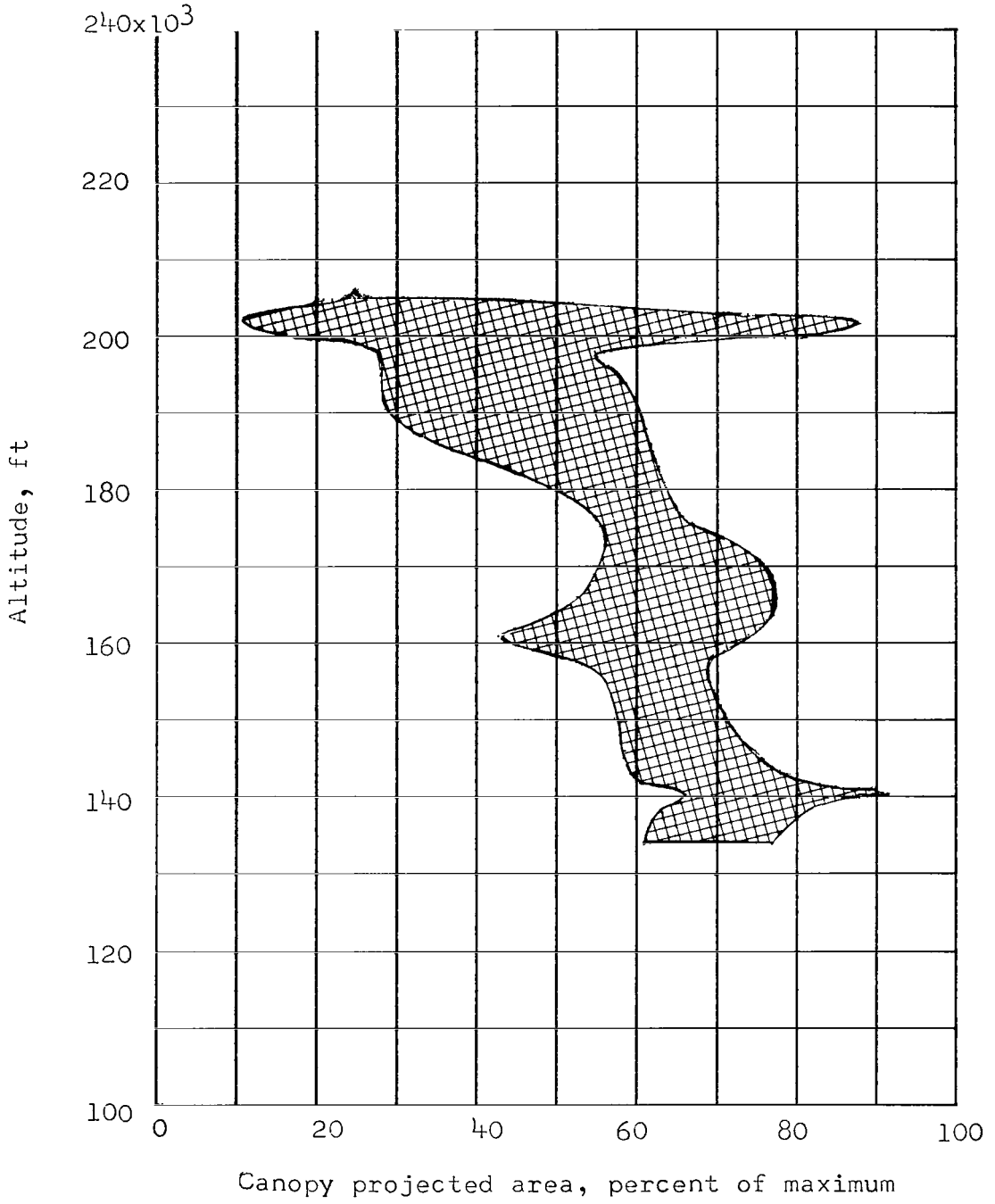

(c) Flight C.

Figure 9.- Concluded.

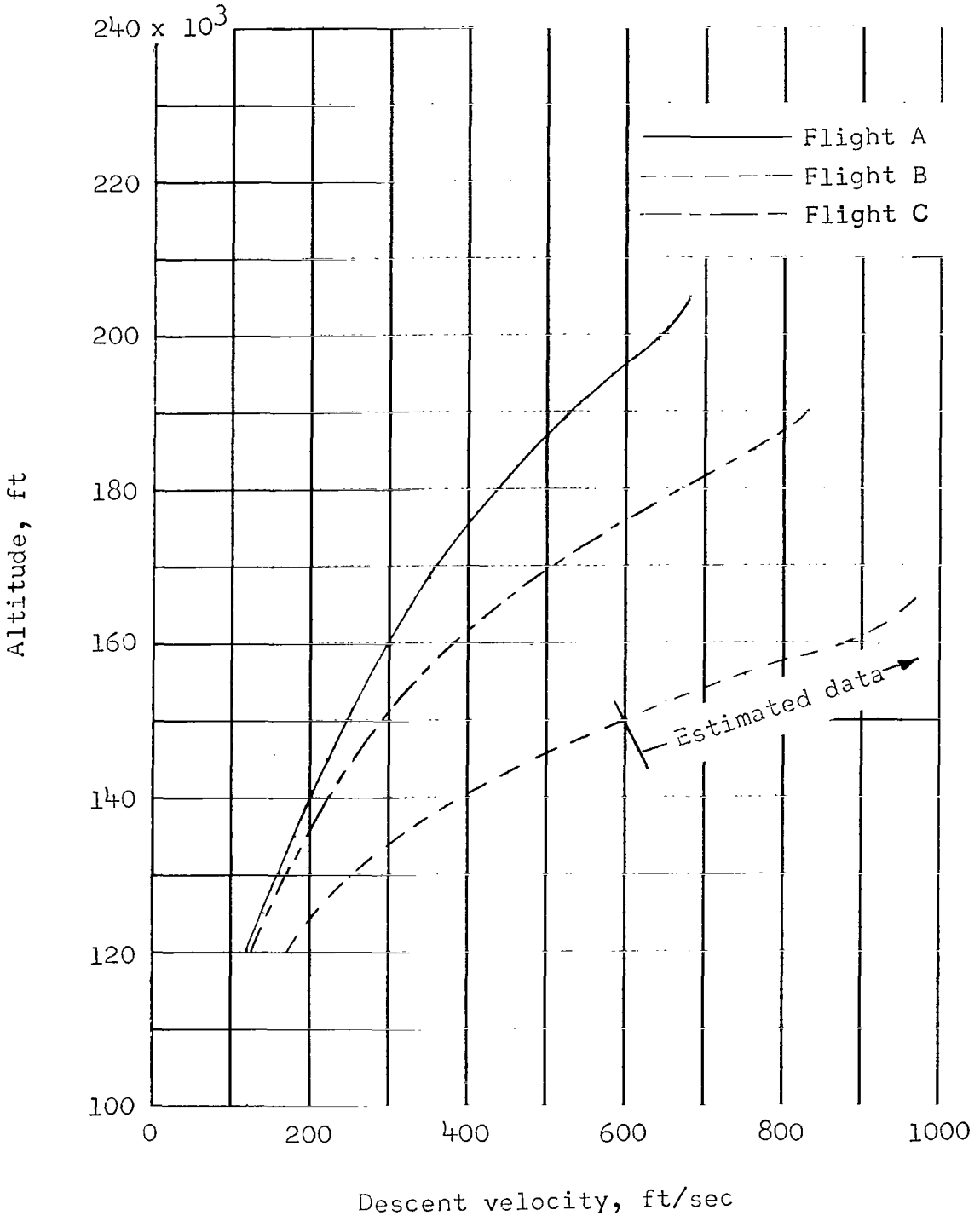

Figure 10.- Variation of descent velocity.

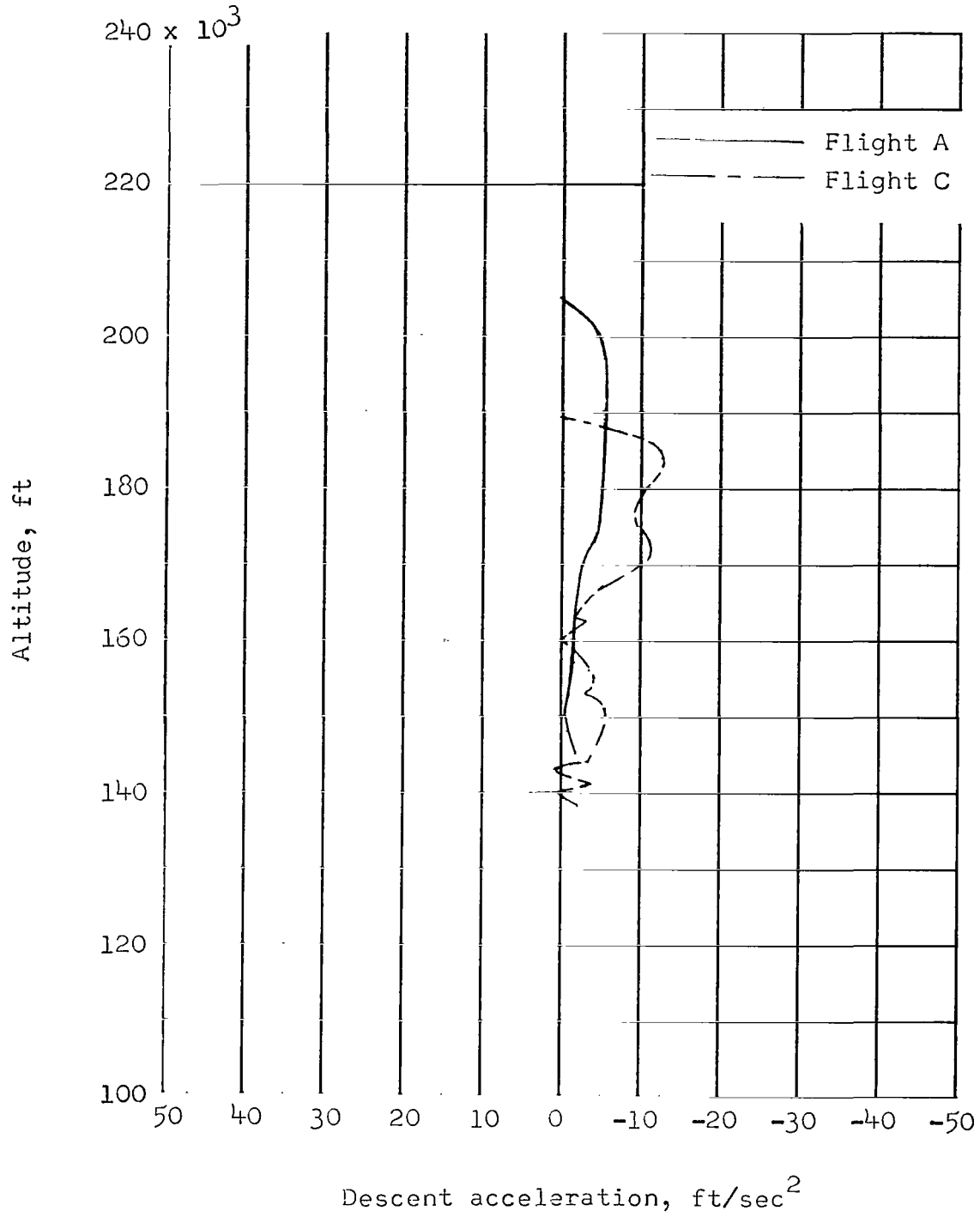

Figure 11.- Variation of descent acceleration.

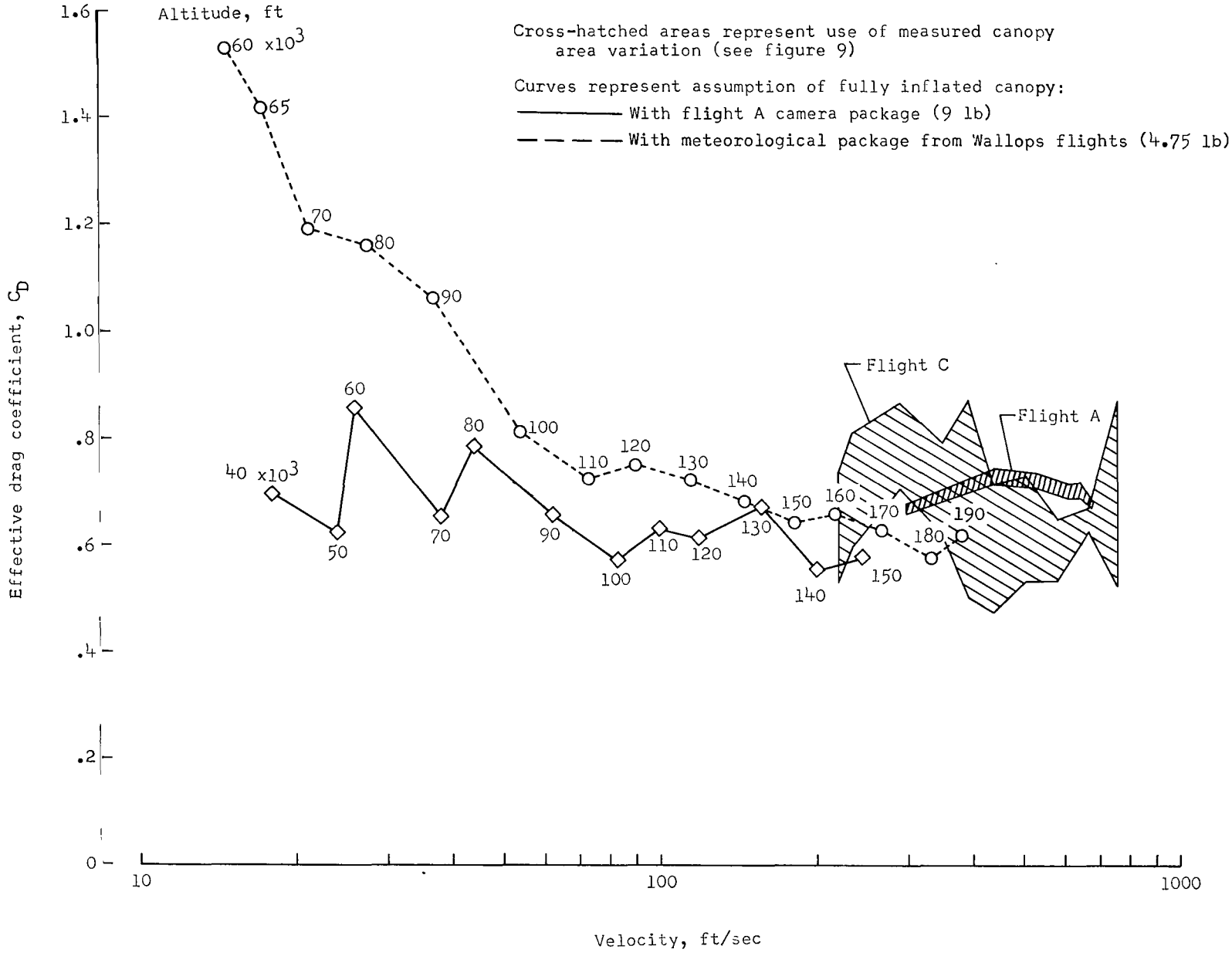

Figure 12.- Variation of effective drag coefficient with velocity.

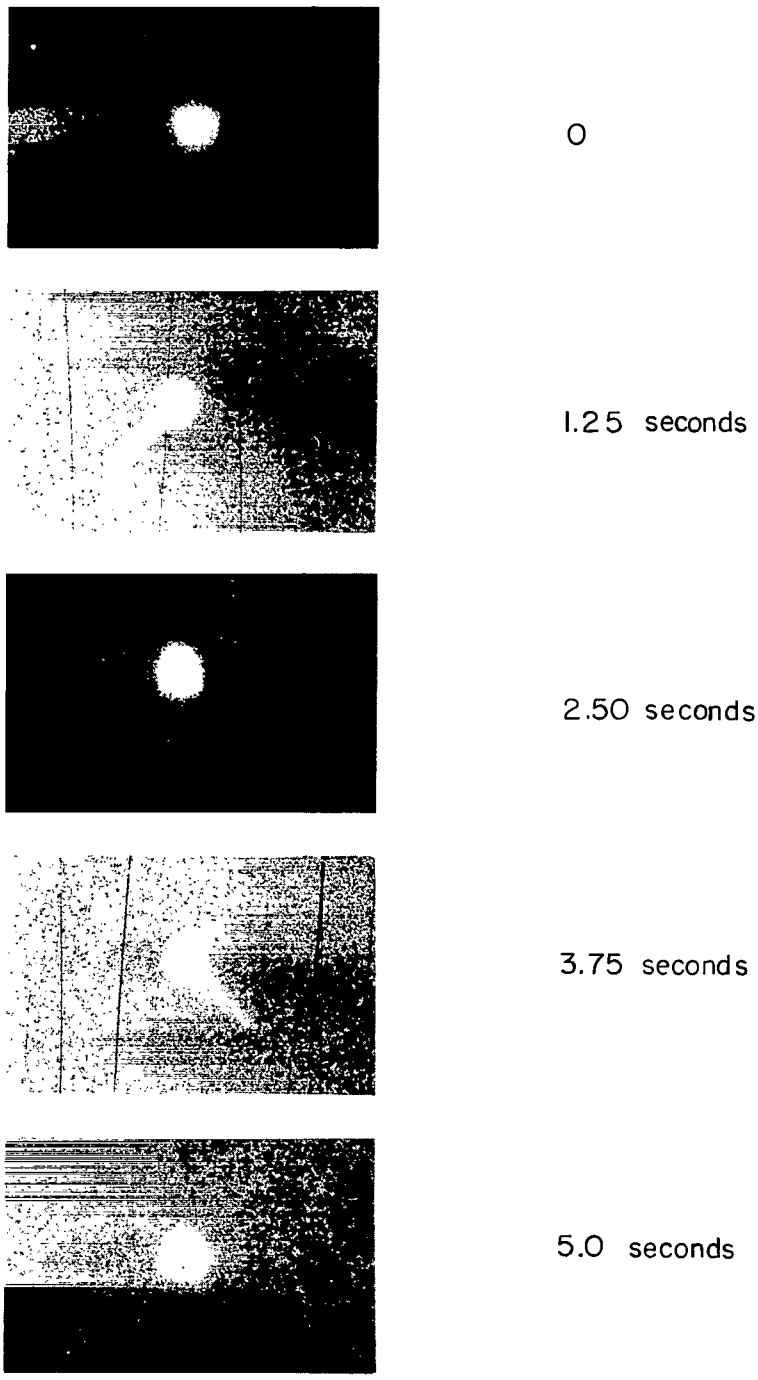

L-63-7523

Figure 13.- Motion-picture sequence of parachute at 150,000 feet. (Taken by ground camera at NASA Wallops Station.)

2/7/05